



# Million-Fold Electrical Conductivity Enhancement in Fe<sub>2</sub>(DEBDC) versus Mn<sub>2</sub>(DEBDC) (E = S, O)

Lei Sun,<sup>†</sup> Christopher H. Hendon,<sup>‡</sup> Mikael A. Minier,<sup>†</sup> Aron Walsh,<sup>‡</sup> and Mircea Dincă<sup>\*,†</sup>

<sup>†</sup>Department of Chemistry, Massachusetts Institute of Technology, Cambridge, Massachusetts 02139, United States

<sup>‡</sup>Department of Chemistry, University of Bath, Claverton Down, Bath BA2 7AY, United Kingdom

## S Supporting Information

**ABSTRACT:** Reaction of FeCl<sub>2</sub> and H<sub>4</sub>DSBDC (2,5-disulfhydrylbenzene-1,4-dicarboxylic acid) leads to the formation of Fe<sub>2</sub>(DSBDC), an analogue of M<sub>2</sub>(DOBDC) (MOF-74, DOBDC<sup>4-</sup> = 2,5-dihydroxybenzene-1,4-dicarboxylate). The bulk electrical conductivity values of both Fe<sub>2</sub>(DSBDC) and Fe<sub>2</sub>(DOBDC) are ~6 orders of magnitude higher than those of the Mn<sup>2+</sup> analogues, Mn<sub>2</sub>(DEBDC) (E = O, S). Because the metals are of the same formal oxidation state, the increase in conductivity is attributed to the loosely bound Fe<sup>2+</sup> β-spin electron. These results provide important insight for the rational design of conductive metal–organic frameworks, highlighting in particular the advantages of iron for synthesizing such materials.

Metal–organic frameworks (MOFs) that display intrinsic electrical conductivity are still rare, but conductivity is emerging as an attractive complement to the inherent porosity of these materials. If high surface area is combined with electrical conductivity or high charge mobility, MOFs could find uses in fields outside traditional areas such as gas storage and separation, and make strides into batteries,<sup>1</sup> supercapacitors,<sup>2</sup> electrocatalysis,<sup>3</sup> and sensing,<sup>4</sup> among others. Although recent reports of conductive MOFs have crystallized several potential avenues toward improved electrical properties, including in-plane π-conjugation,<sup>4,5</sup> through-space charge transport,<sup>6</sup> through-bond charge transport,<sup>7</sup> and doping,<sup>7d,8</sup> these design strategies require significant refinement.

In this context, we recently reported Mn<sub>2</sub>(DSBDC), a MOF-74 analogue that contains (–Mn–S)<sub>∞</sub> chains, and discussed the positive effect of replacing phenoxide by thiophenoxide groups on charge mobility.<sup>7a</sup> While this was inspired by the rich literature of organic conductors, where heavier chalcogens generally lead to better electrical properties,<sup>9</sup> the equally compelling literature of inorganic semiconductors shows, for instance, that iron chalcogenides<sup>10</sup> are better intrinsic conductors than manganese chalcogenides,<sup>11</sup> highlighting that the metal ions may be as important as the chalcogens. Taking a cue from inorganic chalcogenides, we wanted to test the relative importance of the metal ion for MOFs with infinite chains as their secondary building units. To do so, we set out to compare the Mn<sup>2+</sup> and Fe<sup>2+</sup> analogues of the family of materials known as MOF-74, surmising that replacement of Mn<sup>2+</sup> by Fe<sup>2+</sup> would lead to superior electrical conductivity, as seen for the inorganic chalcogenides. Here, we show that within isostructural materials,

replacing Mn<sup>2+</sup> with Fe<sup>2+</sup> leads to a million-fold enhancement in electrical conductivity, a considerably more pronounced effect than substituting bridging O atoms with less electronegative S atoms.

[Fe<sub>2</sub>(DSBDC)(DMF)<sub>2</sub>]<sub>2</sub>·x(DMF) was isolated as dark red-purple crystals after heating a degassed and dry solution of H<sub>4</sub>DSBDC and anhydrous FeCl<sub>2</sub> in *N,N*-dimethylformamide (DMF) at 140 °C under an N<sub>2</sub> atmosphere for 24 h, and washing with additional DMF. Single-crystal X-ray diffraction analysis of Fe<sub>2</sub>(DSBDC)(DMF)<sub>2</sub>·x(DMF) revealed an asymmetric unit containing one Fe atom coordinated by three carboxylate groups, two thiophenoxide groups, and one DMF molecule. The sulfur atoms are coordinated in *trans* fashion to the Fe<sup>2+</sup> atom, with Fe–S bond lengths of 2.444(2) and 2.446(2) Å. This indicates that both S atoms interact with the same d orbital of Fe<sup>2+</sup>, an important orbital symmetry requirement for efficient charge transport.<sup>12</sup> Although Fe<sub>2</sub>(DSBDC) is isostructural with Fe<sub>2</sub>(DOBDC)<sup>13</sup> and Mn<sub>2</sub>(DOBDC),<sup>14</sup> its structure is only topologically related to that of Mn<sub>2</sub>(DSBDC). As shown in Figure 1a, whereas Fe<sub>2</sub>(DSBDC) has a single metal atom in the asymmetric unit, Mn<sub>2</sub>(DSBDC) has two: one that is octahedrally coordinated by donors on DSBDC<sup>4-</sup> ligands, and another that is bound by two DMF molecules. Relevantly, the two distinct metal ions in Mn<sub>2</sub>(DSBDC) reduce the symmetry of the (–Mn–S)<sub>∞</sub> chains, which may negatively affect its charge transport properties. As in other MOF-74 analogues, the (–Fe–S)<sub>∞</sub> chains in Fe<sub>2</sub>(DSBDC) are bridged by thiophenoxide and carboxylate groups to form a three-dimensional framework with one-dimensional hexagonal pores with a van der Waals diameter of ~16 Å (Figures 1b and S1).

When M<sub>2</sub>(DEBDC)(DMF)<sub>2</sub>·x(DMF) are soaked in dichloromethane and then evacuated under vacuum (100 °C, 2 h), they yield M<sub>2</sub>(DEBDC)(DMF)<sub>2</sub>, a series of materials that are guest-free and where DMF completes the coordination sphere of all metal sites. Infrared spectroscopy and microelemental analysis confirmed that all guest solvent molecules were removed under these conditions (Figure S4). Surprisingly, powder X-ray diffraction (PXRD) revealed that Fe<sub>2</sub>(DSBDC)(DMF)<sub>2</sub> is distorted in comparison to Fe<sub>2</sub>(DSBDC)(DMF)<sub>2</sub>·x(DMF), a distortion that was not observed in the other three analogues (Figures S3 and S5). Mathematical simulation and DFT optimization of completely solvent-free Fe<sub>2</sub>(DSBDC)<sup>15</sup> gave a structure whose simulated pattern agreed well with the observed PXRD pattern of Fe<sub>2</sub>(DSBDC)(DMF)<sub>2</sub> (see Figure 1c and the

Received: March 23, 2015

Published: May 1, 2015

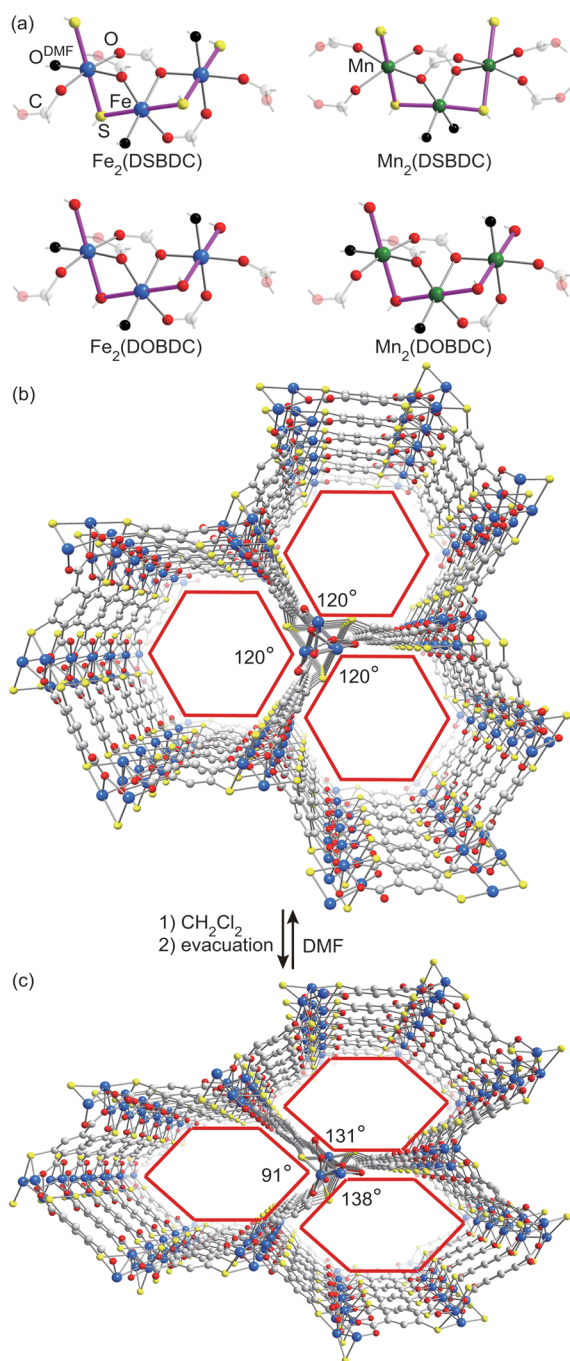


**Figure 1.** (a) Parts of the infinite secondary building units in  $\text{M}_2(\text{DEBDC})(\text{DMF})_2 \cdot x(\text{DMF})$  ( $\text{M} = \text{Fe}, \text{Mn}$ ;  $\text{E} = \text{S}, \text{O}$ ). The  $(-\text{M}-\text{E}-)_{\infty}$  chains are represented in purple. (b,c) Partial structures of  $\text{Fe}_2(\text{DSBDC})(\text{DMF})_2 \cdot x(\text{DMF})$  and  $\text{Fe}_2(\text{DSBDC})(\text{DMF})_2$  as determined by single-crystal X-ray diffraction and DFT structure optimization, respectively. H atoms and solvent molecules are omitted for clarity.

Supporting Information). This distortion is reversible: soaking  $\text{Fe}_2(\text{DSBDC})(\text{DMF})_2$  in fresh DMF produced a crystalline phase with a PXRD pattern identical to that of  $\text{Fe}_2(\text{DSBDC})(\text{DMF})_2 \cdot x(\text{DMF})$  (Figure S6). To our knowledge, although breathing behavior has been observed for several classes of MOFs,<sup>16</sup> it has never been associated with MOF-74 analogues.

$\text{N}_2$  sorption analysis revealed Brunauer–Emmet–Teller (BET) surface areas of 232, 241, and 287  $\text{m}^2/\text{g}$  for  $\text{Mn}_2(\text{DSBDC})(\text{DMF})_2$ ,  $\text{Fe}_2(\text{DOBDC})(\text{DMF})_2$ , and  $\text{Mn}_2(\text{DOBDC})(\text{DMF})_2$ , respectively, confirming their guest-free nature and permanent porosity (Figure S8). These values are lower than those expected for completely activated MOF-74 analogues because coordinated DMF molecules occupy a significant portion of the pore volume in  $\text{M}_2(\text{DEBDC})(\text{DMF})_2$ .  $\text{Fe}_2(\text{DSBDC})(\text{DMF})_2$  exhibited a lower BET surface area of 54  $\text{m}^2/\text{g}$ , likely because the distorted pores in this case are almost entirely occupied by coordinated DMF molecules (Figure S9).

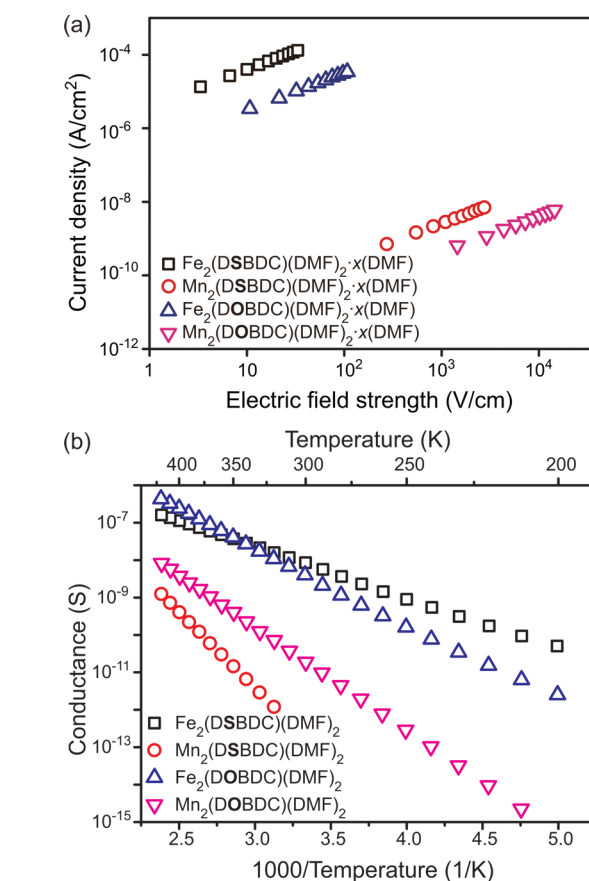


**Figure 2.** Electrical properties of  $\text{M}_2(\text{DEBDC})$  ( $\text{M} = \text{Fe}, \text{Mn}$ ;  $\text{E} = \text{S}, \text{O}$ ) pressed pellets. (a) Plots of current density versus electric field strength ( $J$ – $E$  curves) for  $\text{M}_2(\text{DEBDC})(\text{DMF})_2 \cdot x(\text{DMF})$  at 297 K. (b) Conductance–temperature relationship for  $\text{M}_2(\text{DEBDC})(\text{DMF})_2$ .

Indeed, both  $\text{Fe}_2(\text{DSBDC})(\text{DMF})_2 \cdot x(\text{DMF})$  ( $\sigma = 3.9 \times 10^{-6}$  S/cm) and  $\text{Fe}_2(\text{DOBDC})(\text{DMF})_2 \cdot x(\text{DMF})$  ( $\sigma = 3.2 \times 10^{-7}$  S/cm) were  $\sim 6$  orders of magnitude more conductive than  $\text{Mn}_2(\text{DSBDC})(\text{DMF})_2 \cdot x(\text{DMF})$  and  $\text{Mn}_2(\text{DOBDC})(\text{DMF})_2 \cdot x(\text{DMF})$ , which exhibited conductivities of  $2.5 \times 10^{-12}$  and  $3.9 \times 10^{-13}$  S/cm, respectively (Table 1).<sup>17</sup> Although the guest-free materials showed slightly lower conductivities overall, possibly due to additional defects and grain boundaries caused by the solvent exchange and guest removal process, they reflected the same remarkable 6 orders of

magnitude difference in electrical conductivity between the Fe and Mn analogues, regardless of their solvation level. Indeed, both  $\text{Fe}_2(\text{DSBDC})(\text{DMF})_2 \cdot x(\text{DMF})$  ( $\sigma = 3.9 \times 10^{-6}$  S/cm) and  $\text{Fe}_2(\text{DOBDC})(\text{DMF})_2 \cdot x(\text{DMF})$  ( $\sigma = 3.2 \times 10^{-7}$  S/cm) were  $\sim 6$  orders of magnitude more conductive than  $\text{Mn}_2(\text{DSBDC})(\text{DMF})_2 \cdot x(\text{DMF})$  and  $\text{Mn}_2(\text{DOBDC})(\text{DMF})_2 \cdot x(\text{DMF})$ , which exhibited conductivities of  $2.5 \times 10^{-12}$  and  $3.9 \times 10^{-13}$  S/cm, respectively (Table 1).<sup>17</sup> Although the guest-free materials showed slightly lower conductivities overall, possibly due to additional defects and grain boundaries caused by the solvent exchange and guest removal process, they reflected the same remarkable 6 orders of

**Table 1. Electrical Properties of  $M_2(\text{DEBDC})(\text{DMF})_2$  ( $M = \text{Fe}, \text{Mn}; \text{E} = \text{S}, \text{O}$ )**

	$\text{Fe}_2$ (DSBDC)	$\text{Mn}_2$ (DSBDC)	$\text{Fe}_2$ (DOBDC)	$\text{Mn}_2$ (DOBDC)
$\sigma_{\text{as-synthesized}}$ (S/cm) <sup>a</sup>	$3.9 \times 10^{-6}$	$2.5 \times 10^{-12}$	$3.2 \times 10^{-7}$	$3.9 \times 10^{-13}$
$\sigma_{\text{guest-free}}$ (S/cm) <sup>b</sup>	$5.8 \times 10^{-7}$	$1.2 \times 10^{-12}$	$4.8 \times 10^{-8}$	$3.0 \times 10^{-13}$
$E_a$ (eV) <sup>c</sup>	0.27	0.81	0.41	0.55
$E_g$ (eV) <sup>d</sup>	1.92	2.60	1.47	2.48
$\Phi$ (eV) <sup>e</sup>	3.71	3.81	2.81	3.72

<sup>a</sup>Electrical conductivity of  $M_2(\text{DEBDC})(\text{DMF})_2 \cdot x(\text{DMF})$  at 297 K. <sup>b</sup>Electrical conductivity of  $M_2(\text{DEBDC})(\text{DMF})_2$  at 297 K. <sup>c</sup>Activation energy of  $M_2(\text{DEBDC})(\text{DMF})_2$ . <sup>d</sup>Calculated bandgap of  $M_2(\text{DEBDC})(\text{DMF})_2$ . <sup>e</sup>Calculated work function of  $M_2(\text{DEBDC})(\text{DMF})_2$ .

magnitude difference in conductivity between the Fe and Mn analogues (Table 1). Although at the lower end of intrinsically conductive and porous MOFs, whose conductivity ranges between  $10^{-6}$  and  $10^2$  S/cm,<sup>4–7</sup> the conductivity of the Fe frameworks described here is the highest in the MOF-74 family and is comparable to that of typical organic conductors ( $>10^{-6}$  S/cm).<sup>18</sup>

To probe the cause of the large difference between the Fe and Mn analogues, we determined the activation energy in  $M_2(\text{DEBDC})(\text{DMF})_2$  by measuring their pellet conductance under variable temperature between 200 and 420 K. Working with guest-free rather than as-synthesized materials was necessary because our variable-temperature, air-free electrical microprobe setup requires that samples be passed through an evacuation chamber. However, it is reasonable to assume that because neutral guest solvent molecules are unlikely to contribute to charge transport, the activation energies of  $M_2(\text{DEBDC})(\text{DMF})_2$  are not vastly different and follow the same trends as those of  $M_2(\text{DEBDC})(\text{DMF})_2 \cdot x(\text{DMF})$ . All samples showed an increase in conductance with increasing temperature, indicative of semiconducting behavior (see Figure 2b). Fitting the respective conductance values,  $G$ , to the Arrhenius law (eq 1) revealed notable differences in activation

$$G = G_0 \exp(-E_a/kT) \quad (1)$$

energies,  $E_a$ , shown in Table 1. Thus, both  $\text{Fe}_2(\text{DSBDC})(\text{DMF})_2$  ( $E_a = 0.27$  eV) and  $\text{Fe}_2(\text{DOBDC})(\text{DMF})_2$  ( $E_a = 0.41$  eV) had considerably lower activation energies than  $\text{Mn}_2(\text{DSBDC})(\text{DMF})_2$  ( $E_a = 0.81$  eV) and  $\text{Mn}_2(\text{DOBDC})(\text{DMF})_2$  ( $E_a = 0.55$  eV), suggesting that the Fe-based MOFs have smaller band gaps and hence higher charge density than the Mn-based MOFs.

Notably, the addition of a single electron per metal ion (i.e., substitution of  $d^5$   $\text{Mn}^{2+}$  for  $d^6$   $\text{Fe}^{2+}$ ) has a much more pronounced positive effect on conductivity than changing the bridging atom from O to S, indicating that the electronic structure of the metal ions plays the most important role in charge conduction in this class of materials. To confirm the oxidation state and high-spin configuration of the Fe atoms, we measured  $^{57}\text{Fe}$  Mössbauer spectra of both Fe-based MOFs. As shown in Figures S11 and S12, these spectra revealed well-resolved doublets characterized by isomer shifts of 1.172 and 1.308 mm/s, and quadrupole splittings of 3.218 and 2.739 mm/s, for  $\text{Fe}_2(\text{DSBDC})$  and  $\text{Fe}_2(\text{DOBDC})$ , respectively. Because the isomer shifts of both MOFs fall in the expected range of high-spin

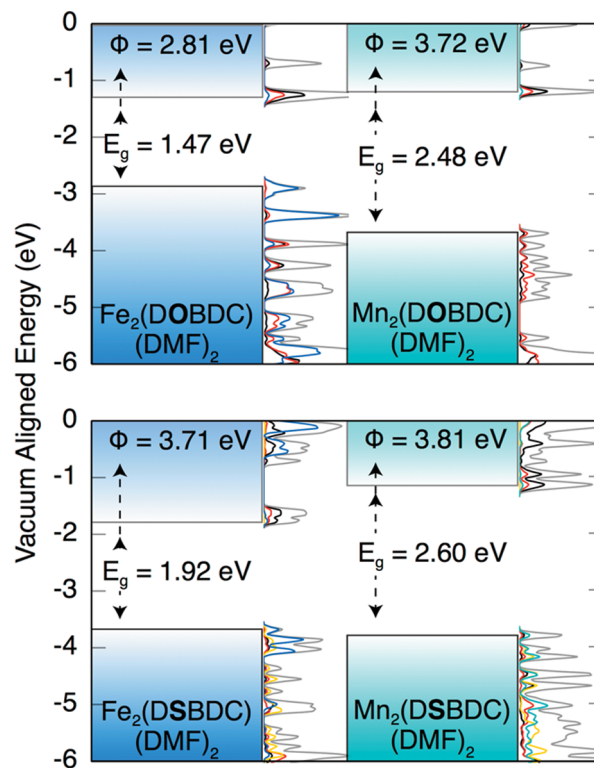


**Figure 3.** Calculated energy bands and projected density of states (DOS) of  $M_2(\text{DEBDC})(\text{DMF})_2$  ( $M = \text{Fe}, \text{Mn}; \text{E} = \text{S}, \text{O}$ ). The work function,  $\Phi$ , and the absolute energy scale are aligned to vacuum according to ref 19. Gray curves represent total DOS. Blue, teal, yellow, red, and black curves represent projected DOS of Fe, Mn, S, O, and C, respectively.

$\text{Fe}^{2+}$ , these experiments demonstrated that oxidation to  $\text{Fe}^{3+}$  did not occur during our experiments.

Density functional calculations were used to further probe the differences in electronic structure of  $M_2(\text{DEBDC})(\text{DMF})_2$ , and the significance of the additional d electron associated with the  $\text{Fe}^{2+}$  ions. The electronic density of states and ionization potentials of the guest-free system are presented in Figure 3, and detailed in the Supporting Information. Because  $\text{Fe}_2(\text{DOBDC})$  and  $\text{Mn}_2(\text{DOBDC})$  are structurally analogous, while  $\text{Fe}_2(\text{DSBDC})$  and  $\text{Mn}_2(\text{DSBDC})$  differ in the number of metal ions in their asymmetric units, the comparison between  $\text{Fe}_2(\text{DOBDC})$  and  $\text{Mn}_2(\text{DOBDC})$  illustrates best the difference between  $\text{Mn}^{2+}$  and  $\text{Fe}^{2+}$ . Most importantly, the valence band maximum of  $\text{Mn}_2(\text{DOBDC})$  is composed of C-p, O-p, and Mn-d states, while in  $\text{Fe}_2(\text{DOBDC})$  the Fe-d states dominate the valence band, with negligible contribution from ligand orbitals. This difference is attributed to the low binding energy of the filled  $\beta$ -spin d band of  $\text{Fe}^{2+}$ , which is empty for the  $d^5$  high-spin  $\text{Mn}^{2+}$  ions.<sup>20</sup> Furthermore, because the lower conduction band in both MOFs is dominated by ligand-based orbitals, the band gaps are narrowed owing to a decreased work function. As a result, the calculated work functions and band gaps of  $\text{Fe}_2(\text{DOBDC})$  are 0.91 and 1.01 eV smaller than those of  $\text{Mn}_2(\text{DOBDC})$ , respectively.

To assess the relative importance of the chalcogen atom on the charge transport, we also compared the structurally analogous  $\text{Fe}_2(\text{DSBDC})$  and  $\text{Fe}_2(\text{DOBDC})$  materials. First, the valence and conduction bands of these frameworks are flat in reciprocal space (dispersion of  $<100$  meV in all cases). This behavior is indicative of localized orbitals rather than delocalized bands, and



is typical of many MOFs.<sup>21</sup> Thus, we anticipate that the primary mode of conduction is through charge hopping. Moreover, because the Fe<sup>2+</sup> d orbitals dominate the valence band (83% of the orbital contribution), intervalence transitions between Fe atoms will proceed with little contribution from O. In contrast, due to the enhanced orbital overlap in Fe<sub>2</sub>(DSBDC), where Fe and S orbitals contribute 53% and 14% to the valence band, transport will occur through both Fe and S in the (-Fe-S)<sub>∞</sub> chains. This mechanism lowers the charge hopping barrier and is also associated with the larger work function of Fe<sub>2</sub>(DSBDC) compared with that of Fe<sub>2</sub>(DOBDC). Finally, the increased contribution of C-p states to the valence band in Fe<sub>2</sub>(DSBDC) compared to Fe<sub>2</sub>(DOBDC) may also indicate a more efficient interchain transport, which further increases the conductivity of the former.

In summary, the synthesis of a new MOF-74 analogue based on (-Fe-S)<sub>∞</sub> chains led to a material with the highest conductivity in the MOF-74 structural family. The combination of loosely bound Fe<sup>2+</sup> β-spin electrons and the low electronegativity of S atoms contributes to the higher relative conductivity of Fe<sub>2</sub>(DSBDC). Applying similar design principles to other MOFs made from one-dimensional secondary building units should lead to further improvements in electrical properties for materials in this class.

## ■ ASSOCIATED CONTENT

### Supporting Information

Experimental details, table of X-ray refinement details, PXRD patterns, IR spectra, I–V curves, Mössbauer spectra, isotherms, computational details, and crystallographic data (CIF). The Supporting Information is available free of charge on the ACS Publications website at DOI: 10.1021/jacs.5b02897.

## ■ AUTHOR INFORMATION

### Corresponding Author

\*mdinca@mit.edu

### Notes

The authors declare no competing financial interest.

## ■ ACKNOWLEDGMENTS

This work was supported by the U.S. Department of Energy, Office of Science, Office of Basic Energy Sciences, under award no. DE-SC0006937. Part of the characterization was performed at the Shared Experimental Facilities, supported by the NSF under the MRSEC Program (DMR-08-19762). M.D. thanks the Sloan Foundation, the Research Corporation for Science Advancement, and 3M for non-tenured faculty awards. Work in the UK benefited from access to ARCHER through membership in the UK's HPC Materials Chemistry Consortium, which is funded by EPSRC (Grant No. EP/L00202). Additional support was received from the European Research Council (Grant No. 277757). We thank Prof. S. J. Lippard for use of the Mössbauer spectrometer and Prof. J. R. Long for valuable discussions.

## ■ REFERENCES

- (1) (a) Férey, G.; Millange, F.; Morcrette, M.; Serre, C.; Doublet, M.; Grenèche, J.; Tarascon, J. *Angew. Chem., Int. Ed.* **2007**, *46*, 3259. (b) Demir-Cakan, R.; Morcrette, M.; Nouar, F.; Davoisne, C.; Devic, T.; Gonbeau, D.; Dominko, R.; Serre, C.; Férey, G.; Tarascon, J. *J. Am. Chem. Soc.* **2011**, *133*, 16154. (c) Wiers, B. M.; Foo, M.; Balsara, N. P.; Long, J. R. *J. Am. Chem. Soc.* **2011**, *133*, 14522. (d) Zhang, Z.; Yoshikawa, H.; Awaga, K. *J. Am. Chem. Soc.* **2014**, *136*, 16112.
- (2) Choi, K. M.; Jeong, H. M.; Park, J. H.; Zhang, Y.; Kang, J. K.; Yaghi, O. M. *ACS Nano* **2014**, *8*, 7451.
- (3) (a) Nohra, B.; Moll, H. E.; Albelo, M. R.; Mialane, P.; Marrot, J.; Mellot-Draznieks, C.; O'Keeffe, M.; Biboum, R. N.; Lemaire, J.; Keita, B.; Nadjo, L.; Dolbecq, A. *J. Am. Chem. Soc.* **2011**, *133*, 13363. (b) Ahrenholtz, S. R.; Epley, C. C.; Morris, A. J. *J. Am. Chem. Soc.* **2014**, *136*, 2464.
- (4) Campbell, M. G.; Sheberla, D.; Liu, S.; Swager, T. M.; Dincă, M. *Angew. Chem., Int. Ed.* **2015**, *54*, 4349.
- (5) (a) Hmadeh, M.; Lu, Z.; Liu, Z.; Gándara, F.; Furukawa, H.; Wan, S.; Augustyn, V.; Chang, R.; Liao, L.; Zhou, F.; Perre, E.; Ozolins, V.; Suenaga, K.; Duan, X.; Dunn, B.; Yamamoto, Y.; Terasaki, O.; Yaghi, O. M. *Chem. Mater.* **2012**, *24*, 3511. (b) Kambe, T.; Sakamoto, R.; Hoshiko, K.; Takada, K.; Miyachi, M.; Ryu, J.; Sasaki, S.; Kim, J.; Nakazato, K.; Takata, M.; Nishihara, H. *J. Am. Chem. Soc.* **2013**, *135*, 2462. (c) Cui, J.; Xu, Z. *Chem. Commun.* **2014**, *50*, 3986. (d) Sheberla, D.; Sun, L.; Blood-Forsythe, M. A.; Er, S.; Wade, C. R.; Brozek, C. K.; Aspuru-Guzik, A.; Dincă, M. *J. Am. Chem. Soc.* **2014**, *136*, 8859.
- (6) (a) Narayan, T. C.; Miyakai, T.; Seki, S.; Dincă, M. *J. Am. Chem. Soc.* **2012**, *134*, 12932. (b) Park, S. S.; Hontz, E. R.; Sun, L.; Hendon, C. H.; Walsh, A.; Van Voorhis, T.; Dincă, M. *J. Am. Chem. Soc.* **2015**, *137*, 1774. (c) Avendano, C.; Zhang, Z.; Ota, A.; Zhao, H.; Dunbar, K. R. *Angew. Chem., Int. Ed.* **2011**, *50*, 6543. (d) Zhang, Z.; Zhao, H.; Kojima, H.; Mori, T.; Dunbar, K. R. *Chem.—Eur. J.* **2013**, *19*, 3348.
- (7) (a) Sun, L.; Miyakai, T.; Seki, S.; Dincă, M. *J. Am. Chem. Soc.* **2013**, *135*, 8185. (b) Gándara, F.; Uribe-Romo, F. J.; Britt, D. K.; Furukawa, H.; Lei, L.; Cheng, R.; Duan, X.; O'Keeffe, M.; Yaghi, O. M. *Chem.—Eur. J.* **2012**, *18*, 10595. (c) Takaishi, S.; Hosoda, M.; Kajiwara, T.; Miyasaka, H.; Yamashita, M.; Nakanishi, Y.; Kitagawa, Y.; Yamaguchi, K.; Kobayashi, A.; Kitagawa, H. *Inorg. Chem.* **2009**, *48*, 9048. (d) Kobayashi, Y.; Jacobs, B.; Allendorf, M. D.; Long, J. R. *Chem. Mater.* **2010**, *22*, 4120.
- (8) (a) Zeng, M.; Wang, Q.; Tan, Y.; Hu, S.; Zhao, H.; Long, L.; Kurmoo, M. *J. Am. Chem. Soc.* **2010**, *132*, 2561. (b) Talin, A. A.; Centrone, A.; Ford, A. C.; Foster, M. E.; Stavila, V.; Haney, P.; Kinney, R. A.; Szalai, V.; Gabaly, F. E.; Yoon, H. P.; Léonard, F.; Allendorf, M. D. *Science* **2014**, *343*, 66.
- (9) Holliday, B. J.; Swager, T. M. *Chem. Commun.* **2005**, 23.
- (10) (a) Fu, G.; Polity, A.; Volbers, N.; Meyer, B. K.; Mogwitz, B.; Janek, J. *Appl. Phys. Lett.* **2006**, *89*, 262113. (b) Park, J.; Kim, D.; Lee, C.; Kim, D. *Bull. Korean Chem. Soc.* **1999**, *20*, 1005.
- (11) (a) Makovetskiĭ, G. I.; Galyas, A. I.; Demidenko, O. F.; Yanushkevich, K. I.; Ryabinkina, L. I.; Romanova, O. B. *Phys. Solid State* **2008**, *50*, 1826. (b) Bhide, V. G.; Dani, R. H. *Physica* **1961**, *27*, 821.
- (12) (a) Anderson, P. W. *Phys. Rev.* **1950**, *79*, 350. (b) Kanamori, J. *J. Phys. Chem. Solids* **1959**, *10*, 87. (c) Tiana, D.; Hendon, C. H.; Walsh, A. *Chem. Commun.* **2014**, *50*, 13990.
- (13) (a) Bhattacharjee, S.; Choi, J.; Yang, S.; Choi, S. B.; Kim, J.; Ahn, W. J. *Nanosci. Nanotechnol.* **2010**, *10*, 135. (b) Bloch, E. D.; Murray, L. J.; Queen, W. L.; Chavan, S.; Maximoff, S. N.; Bigi, J. P.; Krishna, R.; Peterson, V. K.; Grandjean, F.; Long, G. J.; Smit, B.; Bordiga, S.; Brown, C. M.; Long, J. R. *J. Am. Chem. Soc.* **2011**, *133*, 14814.
- (14) (a) Wu, H.; Zhou, W.; Yildirim, T. *J. Am. Chem. Soc.* **2009**, *131*, 4995. (b) Cozzolino, A. F.; Brozek, C. K.; Palmer, R. D.; Yano, J.; Li, M.; Dincă, M. *J. Am. Chem. Soc.* **2014**, *136*, 3334.
- (15) Optimizing Fe<sub>2</sub>(DSBDC)(DMF)<sub>2</sub> itself was computationally unfeasible because the solvent molecules add 72 atoms to the unit cell.
- (16) (a) Barthelet, K.; Marrot, J.; Riou, D.; Férey, G. *Angew. Chem., Int. Ed.* **2002**, *41*, 281. (b) Murdock, C. R.; Hughes, B. C.; Lu, Z.; Jenkins, D. M. *Coord. Chem. Rev.* **2014**, *258–259*, 119.
- (17) J–E curves and log scale are used in Figure 2a to show the difference among conductivities of various MOFs clearly. See Supporting Information.
- (18) Saito, G.; Yoshida, Y. *Top. Curr. Chem.* **2012**, *321*, 67.
- (19) Butler, K. T.; Hendon, C. H.; Walsh, A. *J. Am. Chem. Soc.* **2014**, *136*, 2703.
- (20) Zhang, Q.; Li, B.; Chen, L. *Inorg. Chem.* **2013**, *52*, 9356.
- (21) Butler, K. T.; Hendon, C. H.; Walsh, A. *ACS Appl. Mater. Interfaces* **2014**, *6*, 22044.